8

Transfer Matrices and Periodic Focusing Systems

Periodic focusing channels are used to confine high-energy beams in linear and circular accelerators. Periodic channels consist of a sequence of regions called focusing cells containing one or more charged particle optical elements. A focusing cell is the smallest unit of periodicity in the channel. The main application of periodic channels is in high-energy accelerators that utilize strong focusing. For example, the focusing channel of a linear ion accelerator consists typically of a series of magnetic quadrupole lenses with alternating north-south pole orientation. Thus, along either transverse axis, the lenses are alternately focusing and defocusing. We shall see that such a combination has a net focusing effect that is stronger than a series of solenoid lenses at the same field strength. A quadrupole focusing channel can therefore be constructed with a much smaller bore diameter than a solenoid channel of the same acceptance. The associated reduction in the size and power consumption of focusing magnets has been a key factor in the development of modern high-energy accelerators. Periodic focusing channels also have application at low beam energy. Configurations include the electrostatic accelerator column, the electrostatic Einzel lens array and periodic permanent magnet (PPM) channels used in high-power microwave tubes.

The transfer matrix description of beam transport in near optical elements facilitates the study of periodic focusing channels. The matrix description is a mathematical method to organize information about the transverse motions of particles about the main beam axis. Matrices are particularly helpful when dealing with systems with a large number of different elements. The effects on particles of a single element and combinations of elements are described by the familiar rules of matrix algebra. All the lenses and beam bending devices described in Chapter 6 have associated transfer matrices.

The transfer matrices for the focusing and defocusing axes of a quadrupole lens are derived in Section 8.1. Section 8.2 lists transfer matrices for a variety of common optical elements. The rules for combining matrices to describe complex optical systems are reviewed in Section 8.3. The rules are applied in Section 8.4 to the quadrupole doublet and triplet lenses. These lenses combine quadrupole fields to provide focusing along both transverse axes. Periodic systems are introduced by the example of an array of thin one-dimensional lenses separated by drift spaces (Section 8.5). The discussion illustrates the concepts of phase advance and orbital stability. Matrix algebra is used to extend the treatment to general linear focusing systems. Given the transverse matrix for a focusing cell, the stability limits on beam transport can be derived by studying the mathematical properties of the matrix power operation (Section 8.6). The chapter concludes with a detailed look at orbit stability in a long quadrupole channel (Section 8.7).

8.1 TRANSFER MATRIX OF THE QUADRUPOLE LENS

Transfer matrices describe changes in the transverse position and angle of a particle relative to the main beam axis. We assume paraxial motion and linear fields. The axial velocity v_z and the location of the main axis are assumed known by a previous equilibrium calculation. If x and y are the coordinates normal to z, then a particle orbit at some axial position can be represented by the four-dimensional vector (x, x', y, y'). In other words, four quantities specify the particle orbit. The quantities x' and y' are angles with respect to the axis; they are equivalent to transverse velocities if v_z is known. We further assume that the charged particle optical system consists of a number of separable focusing elements. Separable means that boundary planes between the elements can be identified. We seek information on orbit vectors at the boundary planes and do not inquire about details of the orbits within the elements. In this sense, an optical element operates on an entrance orbit vector to generate an output orbit vector. The transfer matrix represents this operation.

Orbits of particles in a magnetic quadrupole lens were discussed in Section 6.10. The same equations describe the electric quadrupole with a correct choice of transverse axes and the replacement $\kappa_m \Rightarrow \kappa_e$. In the following discussion, κ can represent either type of lens. According to Eqs. (6.31) and (6.32), motions in the x and y directions are separable. Orbits can therefore be represented by two independent two-dimensional vectors, $\boldsymbol{u} = (x, x')$ and $\boldsymbol{v} = (y, y')$. This separation holds for other useful optical elements, such as the magnetic sector field (Section 6.8) and the focusing edge (Section 6.9). We shall concentrate initially on analyses of orbits along one coordinate. Orbit vectors have two components and transfer matrices have dimensions 2×2.

Consider motion in the x direction in a quadrupole lens oriented as shown in Figure 5.16. The lens is focusing in the x direction. If the lens has a length l, the exit parameters are related to the entrance parameters by

$$x_f = x_i \cos(\sqrt{\kappa}l) + x_i' \sin(\sqrt{\kappa}l)/\sqrt{\kappa}, \qquad (8.1)$$

$$x_f' = -x_i \sqrt{\kappa} \sin(\sqrt{\kappa}l) + x_i' \cos(\sqrt{\kappa}l). \qquad (8.2)$$

The lens converts the orbit vector $\boldsymbol{u}_i = (x_i, x_i')$ into the vector $\boldsymbol{u}_f = (x_f, x_f')$. The components of $\boldsymbol{u}_f$ are linear combinations of the components of $\boldsymbol{u}_i$. The operation can be written in matrix notation as

$$\boldsymbol{u_f} = \boldsymbol{A_F}\, \boldsymbol{u_i}, \qquad (8.3)$$

if $\boldsymbol{A}_F$ is taken as

$$\boldsymbol{A_F} = \begin{bmatrix} \cos(\sqrt{\kappa}l) & \sin(\sqrt{\kappa}l)/\sqrt{\kappa} \\ -\sqrt{\kappa}\sin(\sqrt{\kappa}l) & \cos(\sqrt{\kappa}l) \end{bmatrix}, \qquad (8.4)$$

where the subscript F denotes the focusing direction. For review, the rule for multiplication of a 2 × 2 matrix times a vector is

$$\begin{bmatrix} a_{11} & a_{12} \\ a_{21} & a_{22} \end{bmatrix} \begin{pmatrix} x \\ x' \end{pmatrix} = \begin{pmatrix} a_{11}x + a_{12}x' \\ a_{21}x + a_{22}x' \end{pmatrix}. \qquad (8.5)$$

If the poles in Figure 5.16 are rotated 90°, the lens defocuses in the x direction. The transfer matrix in this case is

$$\boldsymbol{A_D} = \begin{bmatrix} \cosh(\sqrt{\kappa}l) & \sinh(\sqrt{\kappa}l)/\sqrt{\kappa} \\ \sqrt{\kappa}\sinh(\sqrt{\kappa}l) & \cosh(\sqrt{\kappa}l) \end{bmatrix}, \qquad (8.6)$$

Quadrupole lenses are usually used in the limit $\sqrt{\kappa}\; l \leq 1$. In this case, the trigonometric and hyperbolic functions of Eqs. (8.4) and (8.6) can be expanded in a power series. For reference, the power series forms for the transfer matrices are

$$\boldsymbol{A_F} = \begin{bmatrix} 1-\Gamma^2/2+\Gamma^4/24+\ldots & (\Gamma-\Gamma^3/6+\ldots)/\sqrt{\kappa} \\ -\sqrt{\kappa}(\Gamma-\Gamma^3/6+\ldots) & 1-\Gamma^2/2+\Gamma^4/24+\ldots \end{bmatrix}, \qquad (8.7)$$

and

$$\boldsymbol{A_D} = \begin{bmatrix} 1+\Gamma^2/2+\Gamma^4/24+... & (\Gamma+\Gamma^3/6+...)/\sqrt{\kappa} \\ \sqrt{\kappa}(\Gamma+\Gamma^3/6+...) & 1+\Gamma^2/2+\Gamma^4/24+... \end{bmatrix}, \tag{8.8}$$

where $\Gamma = \sqrt{\kappa}l$. The example of the quadrupole illustrates the method for finding the transfer matrix for a linear optical element. Numerical or analytic orbit calculations lead to the identification of the four matrix components. The transfer matrix contains complete information on the properties of the lens as an orbit operator.

When the action of a focusing system is not decoupled in x and y, the full four-dimensional vector must be used and the transfer matrices have the form

$$\begin{bmatrix} \blacksquare & \blacksquare & \square & \square \\ \blacksquare & \blacksquare & \square & \square \\ \square & \square & \blacksquare & \blacksquare \\ \square & \square & \blacksquare & \blacksquare \end{bmatrix}.$$

A focusing system consisting of quadrupole lenses mixed with axisymmetric elements (such as solenoid lens) has coupling of x and y motions. The transfer matrix for this system has coupling components represented by the open boxes above. Sometimes, in the design of particle spectrometers (where beam energy spread is of prime concern), an extra dimension is added to the orbit vector to represent chromaticity, or the variations of orbit parameters with energy [see P. Dahl, **Introduction to Electron and Ion Optics** (Academic Press, New York, 1973) Chapter 2] In this case, the orbit vector is represented as $\boldsymbol{u} = (x, x', y, y', T)$.

8 .2 TRANSFER MATRICES FOR COMMON OPTICAL ELEMENTS

The following examples illustrate the concept of ray transfer matrices and indicate how they are derived. The simplest case is the thin one-dimensional lens, illustrated in Figure 8.1. Only the angle of the orbit changes when a particle passes through the lens. Following Section 6.4, the transformation of orbit variables is

$$x_f = x_i, \qquad x_f' - x_i' - x/f, \tag{8.9}$$

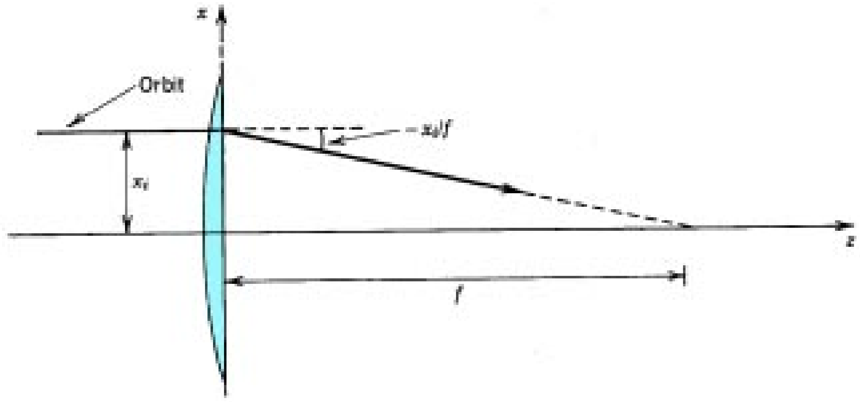

Figure 8.1 Effect of a thin lens (focal length f) on a particle orbit initially parallel to the axis.

where *f* is the focal length. This can be written in the form of Eq. (8.3) with the transfer matrix,

$$\mathbf{A} = \begin{bmatrix} 1 & 0 \\ -1/f & 1) \end{bmatrix}. \tag{8.11}$$

The matrix for a diverging lens is the same except for the term a_{21} which equals $+1/f$. In general, the sign of a_{21} indicates whether the optical element (or combination of elements) is focusing or defocusing.

An optical element is defined as any region in a focusing system that operates on an orbit vector to change the orbit parameters. Thus, there is a transfer matrix associated with translation in field-free space along the z axis (Fig. 8.2). In this case, the distance from the axis changes according to $x_f = x_i + x_i' d$, where *d* is the length of the drift space. The angle is unchanged. The transfer matrix is

$$\mathbf{A} = \begin{bmatrix} 1 & d \\ 0 & 1) \end{bmatrix}. \tag{8.12}$$

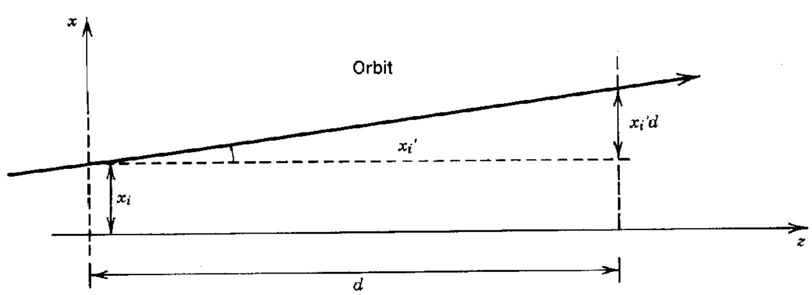

Figure 8.2 Modification of a particle orbit passing through a drift region of length d.

We have already studied the magnetic sector lens with uniform field (Section 6.8). A gradient can be added to the sector field to change the focal properties by varying the width of the gap, as shown in Figure 8.3. Consider the following special case. The magnet has boundaries perpendicular to the main orbit so that there is no edge focusing. Furthermore, the field gradient is parallel to the radius of curvature of the main orbit. With these assumptions, the sector field of Figure 8.3 is a pie-shaped segment of the betatron field studied in Section 7.3. The field variation near the main radius is characterized by the field index n_o [Eq. (7.18)]. Motions about the main axis in the horizontal and vertical direction are decoupled and are described by independent 2 × 2 matrices. Applying Eq. (7.30), motion in the horizontal plane is given by

$$x = A\ \cos[\sqrt{1-n_o}\ (z/r_g) + \varphi], \qquad (8.12)$$

$$x = dx/dz = -[\sqrt{1-n_o}/r_g]\ A\ \sin[\sqrt{1-n_o}\ (z/r_g) + \varphi]. \qquad (8.13)$$

The initial position and angle are related to the amplitude and phase by $x_i = A\cos\varphi$ and $x_i^{/} = -\sqrt{1-n_o}\ A\ \sin\varphi/r_g$. In order to determine the net effect of a sector (with transit distance $-d = \alpha r_g$) on horizontal motion, we consider two special input vectors, $(x_i, 0)$ and $(0, x_i')$. In the first case $\varphi = 0$ and in the second $\varphi = \pi/2$. According to Eqs. (8.12) and (8.13), the final orbit parameters for a particle entering parallel to the main axis are

$$x_f = x_i\ \cos(\sqrt{1-n_o}\ d\ /\ r_g), \qquad (8.14)$$

and

$$x_f^{/} = -x_i\ (\sqrt{1-n_o}/r_g)\ \sin(\sqrt{1-n_o}\ d\ /\ r_g), \qquad (8.15)$$

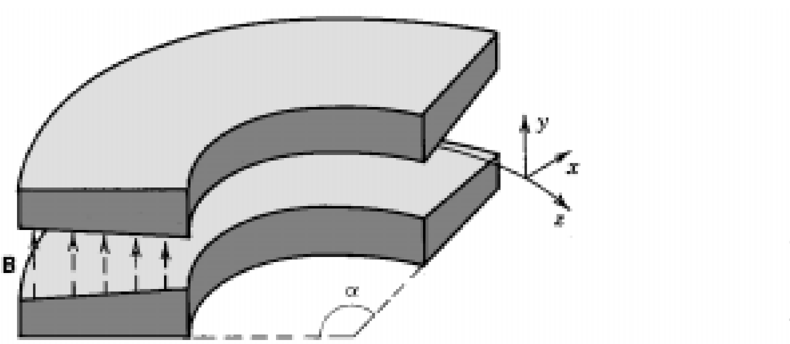

Figure 8.3 Sector magnet of angular extent α with a negative field gradient along the radius of curvature of the main particle orbit.

Similarly, if the particle enters on the main axis at an angle, the final orbit parameters are

$$x_f = x_i' \; r_g \; \sin(\sqrt{1-n_o} \; d \,/\, r_g) \,/\, \sqrt{1-n_o} \,, \tag{8.16}$$

and

$$x_f' = x_i' \; \cos(\sqrt{1-n_o} \; d \,/\, r_g). \tag{8.17}$$

The factor d/r_g is equal to α, the angle subtended by the sector. Combining the results of Eqs. (8.14)-(8.17), the transfer matrix is

$$\boldsymbol{A_H} = \begin{bmatrix} \cos(\sqrt{1-n_o} \; \alpha) & r_g \sin(\sqrt{1-n_o} \; \alpha)/\sqrt{1-n_o} \\ -\sqrt{1-n_o} \; \sin(\sqrt{1-n_o} \; \alpha)/r_g & \cos(\sqrt{1-n_o} \; \alpha) \end{bmatrix}. \tag{8.18}$$

Similarly, for the vertical direction,

$$\boldsymbol{A_V} = \begin{bmatrix} \cos(\sqrt{n_o} \; \alpha) & r_g \sin(\sqrt{n_o} \; \alpha)/\sqrt{n_o} \\ -\sqrt{n_o} \; \sin(\sqrt{n_o} \; \alpha)/r_g & \cos(\sqrt{n_o} \; \alpha) \end{bmatrix}. \tag{8.19}$$

Following the development of Section 6.8, initially parallel beams are focused in the horizontal direction. The focal point is located a distance

$$f' = r_g/\tan(\sqrt{1-n_o} \; \alpha) \tag{8.20}$$

beyond the sector exit. This should be compared to Eq. (6.27). When n_o is negative (a positive field gradient moving out along the radius of curvature), horizontal focusing is strengthened. Conversely, a positive field index decreases the horizontal focusing. There is also vertical focusing when the field index is positive. The distance to the vertical focal point is

$$f' = r_g/\tan(\sqrt{n_o} \; \alpha) \tag{8.21}$$

If $n_o = +0.5$, horizontal and vertical focal lengths are equal and the sector lens can produce a two-dimensional image. The dual-focusing property of the gradient field is used in charged particle spectrometers.

Particles may travel in either direction through a sector magnet field, so there are two transfer matrices for the device. The matrix for negatively directed particles can be calculated directly. The transfer matrix for particles moving backward in the sector field is the *inverse* of the matrix for forward motion. The inverse of a 2 × 2 matrix

$$\boldsymbol{A} = \begin{bmatrix} a_{11} & a_{12} \\ a_{21} & a_{22} \end{bmatrix}$$

is

$$\boldsymbol{A} = \frac{1}{\det\boldsymbol{A}} \begin{bmatrix} a_{22} & -a_{12} \\ -a_{21} & a_{11} \end{bmatrix}. \tag{8.22}$$

The quantity ***detA*** is the determinant of the matrix ***A***, defined by

$$\det\boldsymbol{A} = a_{11}a_{22} - a_{12}a_{21}. \tag{8.23}$$

The determinant of the sector field transfer matrix in the horizontal direction is equal to 1. The inverse is

$$\boldsymbol{A}_{\boldsymbol{H}}^{-\mathbf{1}} = \begin{bmatrix} \cos(\sqrt{1-n_o}\ \alpha) & -r_g\sin(\sqrt{1-n_o}\ \alpha)/\sqrt{1-n_o} \\ \sqrt{1-n_o}\ \sin(\sqrt{1-n_o}\ \alpha)/r_g & \cos(\sqrt{1-n_o}\ \alpha) \end{bmatrix}. \tag{8.24}$$

Equation (8.24) is equal to Eq. (8.18) with the replacement $\alpha \Rightarrow -\alpha$. The negative angle corresponds to motion in the -*z* direction. The effect of the element is independent of the direction. The same holds true for any optical element in which the energy of the charged particle is unchanged. We can verify that in this case ***detA*** = 1.

Acceleration gaps in linear accelerators have the geometry of the immersion lens (Figure 6.10). This lens does not have the same focal properties for particle motion in different directions. Assume the focal length for motion of nonrelativistic particles in the accelerating direction, f_a, is known. This is a function of the lens geometry as well as the absolute potentials of each of the tubes. The upstream potential is $\varphi_1$while the downstream potential is φ_2. The quantity ξ is defined as the ratio of the exit velocity to the entrance velocity and is equal to $\xi = \sqrt{\varphi_2/\varphi_1}$. In the thin-lens approximation, a particle's position is constant but the transverse angle is changed. If the particle entered parallel to the axis in the accelerating direction, it would emerge at an angle $-x_i/f_a$. Similarly, a particle with an entrance vector $(0, x_i')$ emerges at an angle x_i'/ξ. The traverse velocity is the same, but the longitudinal velocity increases. The general form for the transfer matrix of a thin electrostatic lens with acceleration is

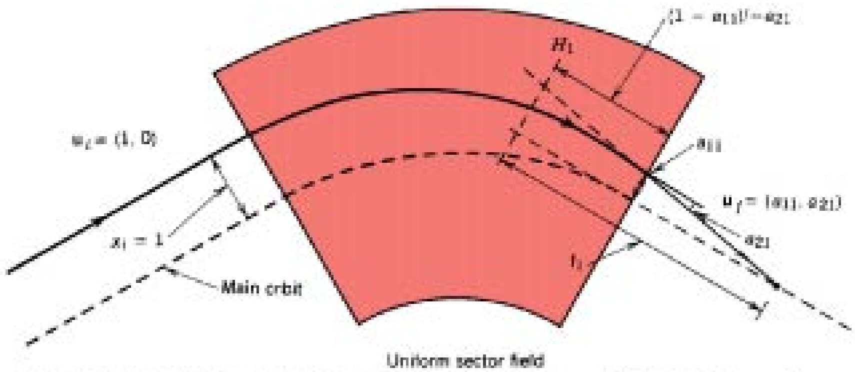

Figure 8.4 Horizontal particle motion in a uniform-field sector magnet. Relationship between the elements of the transfer matrix and the principal planes and focal lengths of Gaussian optics.

$$\boldsymbol{A} = \begin{bmatrix} 1 & 0 \\ -1/f_a & 1/\xi \end{bmatrix}. \tag{8.25}$$

The determinant has the value $\det\boldsymbol{A} = 1/\xi \neq 1$. The transfer matrix for a decelerating lens is the inverse of $\boldsymbol{A}$. Applying Eq. (8.22) and inverting signs so that the particle travels in the $+z$ direction,

$$\boldsymbol{A} = \begin{bmatrix} 1 & 0 \\ -\xi/f_a & \xi \end{bmatrix}. \tag{8.26}$$

In the thin-lens limit, the accelerating and decelerating focal lengths are related by $f_d = f_a/\xi$.

To conclude the discussion of transfer matrices, we consider how the four components of transfer matrices are related to the focal lengths and principal planes of Gaussian optics (Chapter 6). Consider the uniform sector field of Figure 8.4. This acts as a thick lens with a curved main axis. An orbit vector *(1, 0)* is incident from the left. The relationship between the emerging orbit and the matrix components as well as the focal length and principal plane H_1 are indicated on the figure. Applying the law of similar triangles, the focal length is given by $f_1 = -l/a_{11}$. The principal plane is located a distance $z_1 = (1 - a_{11})/a_{21}$ from the boundary. Thus, the components a_{11} and a_{21} are related to f_1 and H_1. When the matrix is inverted, the components a_{12} and a_{22} move to the first column. They are related to f_2 and H_2 for particles traveling from right to left. The matrix and Gaussian descriptions of linear lenses are equivalent. Lens properties are completely determined by four quantities.

8.3 COMBINING OPTICAL ELEMENTS

Matrix algebra makes it relatively easy to find the cumulative effect of a series of transport devices. A single optical element operates on an entrance orbit vector, $\boldsymbol{u}_0$, changing it to an exit vector, $\boldsymbol{u}_1$. This vector may be the entrance vector to another element, which subsequently changes it to $\boldsymbol{u}_2$. By the superposition property of linear systems, the combined action of the two elements can be represented by a single matrix that transforms $\boldsymbol{u}_0$ directly to $\boldsymbol{u}_2$.

If **A** is the transfer matrix for the first element and **B** for the second, the process can be written symbolically,

$$\boldsymbol{u}_1 = \boldsymbol{A}\ \boldsymbol{u}_0, \qquad \boldsymbol{u}_2 = \boldsymbol{B}\ \boldsymbol{u}_1 = \boldsymbol{B}\ (\boldsymbol{A}\ \boldsymbol{u}_0),$$

or

$$\boldsymbol{u}_2 = \boldsymbol{C}\ \boldsymbol{u}_0.$$

The matrix **C** is a function of **A** and **B**. The functional dependence is called *matrix multiplication* and is denoted **C** = **BA**. The rule for multiplication of two 2 × 2 matrices is

$$\boldsymbol{C} = \begin{bmatrix} c_{11} & c_{12} \\ c_{21} & c_{22} \end{bmatrix} = \begin{bmatrix} b_{11} & b_{12} \\ b_{21} & b_{22} \end{bmatrix} \begin{bmatrix} a_{11} & a_{12} \\ a_{21} & a_{22} \end{bmatrix}, \tag{8.27}$$

where

$$c_{11} = b_{11}a_{11} + b_{12}a_{21}, \qquad c_{12} = b_{11}a_{12} + b_{12}a_{22},$$

$$c_{21} = b_{21}a_{11} + b_{22}a_{21}, \qquad c_{22} = b_{21}a_{21} + b_{22}a_{22}.$$

We shall verify the validity of Eq. (8.27) for the example illustrated in Figure 8.5. The optical

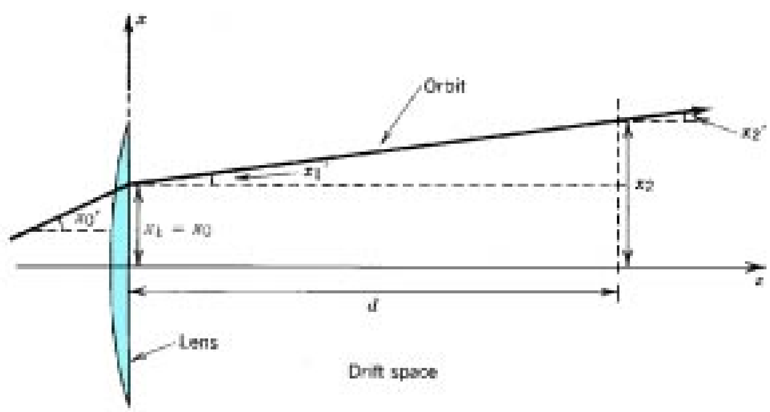

Figure 8.5 Orbit of a particle passing through a thin lens of focal length *f* and along a drift distance *d*.

system consists of two one-dimensional elements, a thin lens with focal length *f* followed by a drift space *d*. The particle entrance orbit is (x_0, x_0'). The position and angle emerging from the lens are $x_1 = x_0$ and $x_1' = x_0' - x_0/f$. Traveling through the drift space, the orbit angle remains constant but the displacement changes by an amount $\Delta x = x_1'd$. The total transformation is

$$x_2 = x_0 + (x_0' - x_0/f)\, d = x_0\, (1 - d/f) = x_o'd, \tag{8.28}$$

$$x_2' = x_0' - x_0/f. \tag{8.29}$$

Inspection of Eqs. (8.28) and (8.29) yields the 2 × 2 transformation matrix,

$$\boldsymbol{C} = \begin{bmatrix} 1-d/f & d \\ -1/f & 1 \end{bmatrix} = \begin{bmatrix} 1 & d \\ 0 & 1 \end{bmatrix} \begin{bmatrix} 1 & 0 \\ -1/f & 1 \end{bmatrix}. \tag{8.30}$$

We can easily verify that **C** is the matrix product of Eq. (8.11) by Eq. (8.10).

It is important to note that the mathematic order of matrix multiplication must replicate the geometric order in which the elements are encountered. Matrix multiplication is not commutative, so that **AB** ≠ **BA**. The inequality can be demonstrated by calculating the transfer matrix for a drift space followed by a lens. The effect of this combination is not the same as a lens followed by a drift space. Consider a parallel orbit entering the two systems. In the drift-lens geometry, the particle emerges at the same position it entered. In the second combination, the final position will be different. Multiplying transfer matrices in the improper order is a frequent source of error. To reiterate, if a particle travels in sequence through elements represented by $\mathbf{A}_1$, $\mathbf{A}_2$, ... , $\mathbf{A}_{n-1}$, $\mathbf{A}_n$, then the combination of these elements is a matrix given by

$$\boldsymbol{C} = \boldsymbol{A}_n\, \boldsymbol{A}_{n-1}\, \dots\, \boldsymbol{A}_2\, \boldsymbol{A}_1. \tag{8.31}$$

The astigmatic focusing property of quadrupole doublets (Section 8.4) is an important consequence of the noncommutative property of matrix multiplication.

We can use matrix algebra to investigate the imaging property of a one-dimensional thin lens. The proof that a thin lens can form an image has been deferred from Section 6.4. The optical system consists of a drift space of length d_2, a lens with focal length *f* and another drift space d_1 (see Fig. 6.7). The vectors (x_0, x_0') and (x_3, x_3') represent the orbits in the planes σ_1 and σ_2. The planes are object and image planes if all rays that leave a point in σ_1 pass through a corresponding point in σ_2, regardless of the orbit angle. An equivalent statement is that x_3 is a function of x_0 with no dependence on x_0'. The transfer matrix for the system is

$$\boldsymbol{C} = \begin{bmatrix} 1 & d_1 \\ 0 & 1 \end{bmatrix} \begin{bmatrix} 1 & 0 \\ -1/f & 1 \end{bmatrix} \begin{bmatrix} 1 & d_2 \\ 0 & 1 \end{bmatrix}$$
$$= \begin{bmatrix} 1-d_1/f & d_1+d_2-d_1d_2/f \\ -1/f & 1-d_2/f \end{bmatrix}. \quad (8.32)$$

The position of the output vector in component form is $x_3 = c_{11}x_0 + c_{12}x_0'$. An image is formed if $c_{12} = 0$. This is equivalent to $1/f = (1/d_1) + (1/d_2)$. This is the thin-lens formula of Eq. (6.15). When the image condition holds, $M = x_2/x_1 = c_{11}$.

8.4 QUADRUPOLE DOUBLET AND TRIPLET LENSES

A quadrupole lens focuses in one coordinate direction and defocuses in the other. A single lens cannot be used to focus a beam to a point or to produce a two-dimensional image. Two-dimensional focusing can be accomplished with combinations of quadrupole lenses. We will study the focal properties of two (doublets) and three quadrupole lenses (triplets). Quadrupole lens combinations form the basis for most high-energy particle transport systems. They occur as extended arrays or as discrete lenses for final focus to a target. Quadrupole lens combinations are convenient to describe since transverse motions are separable in *x* and *y* if the poles (electrodes) are aligned with the axes as shown in Figures 4.14 (for the electrostatic lens) and 5.16 (for the magnetic lens). A 2 × 2 matrix analysis can be applied to each direction.

The magnetic quadrupole doublet is illustrated in Figure 8.6. We shall consider identical lenses in close proximity, neglecting the effects of gaps and edge fields. It is not difficult to extend the treatment to a geometry with a drift space between the quadrupoles. Relative to the *x* direction,

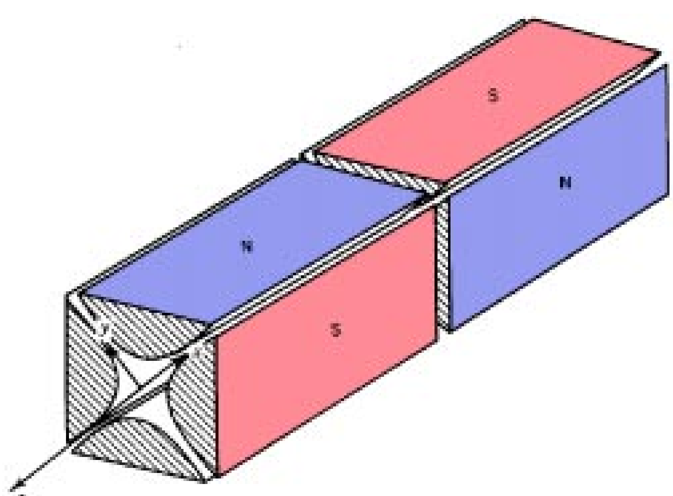

Figure 8.6 Magnetic quadrupole doublet lens.

the first element is focusing and the second is defocusing. This is represented symbolically as

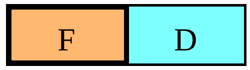

where particles move from left to right. Conversely, in the y direction the doublet is denoted

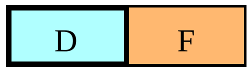

The transfer matrices for the combination of the two elements can be found by matrix multiplication of Eqs. (8.4) and (8.6). The multiplication must be performed in the proper order. The result for an *FD* channel is

$$\boldsymbol{C_{FD}} = \begin{bmatrix} \cos\Gamma\cosh\Gamma - \sin\Gamma\sinh\Gamma & (\cosh\Gamma\sin\Gamma + \cos\Gamma\sinh\Gamma)/\sqrt{\kappa} \\ \sqrt{\kappa}(\cos\Gamma\sinh\Gamma - \cosh\Gamma\sin\Gamma) & \cos\Gamma\cosh\Gamma + \sin\Gamma\sinh\Gamma \end{bmatrix}. \tag{8.33}$$

where $\Gamma = \sqrt{\kappa}l$. Similarly, for a *DF* channel,

$$\boldsymbol{C_{DF}} = \begin{bmatrix} \cos\Gamma\cosh\Gamma + \sin\Gamma\sinh\Gamma & (\cosh\Gamma\sin\Gamma + \cos\Gamma\sinh\Gamma)/\sqrt{\kappa} \\ \sqrt{\kappa}(\cos\Gamma\sinh\Gamma - \cosh\Gamma\sin\Gamma) & \cos\Gamma\cosh\Gamma - \sin\Gamma\sinh\Gamma \end{bmatrix}. \tag{8.34}$$

Equations (8.33) and (8.34) have two main implications. First, the combination of equal defocusing and focusing elements leads to net focusing, and, second, focusing is different in the *x* and *y* directions. As we found in the previous section, the term c_{21} of the transfer matrix determines whether the lens is focusing or defocusing. In this case, $c_{21} = \sqrt{\kappa}\ (\cos\sqrt{\kappa}l\sinh\sqrt{\kappa}l - \cosh\sqrt{\kappa}l\sin\sqrt{\kappa}l)$. We can verify by direct computation that $c_{21} = 0$ at $\sqrt{\kappa}l = 0$ and it is a monotonically decreasing function for all positive values of $\sqrt{\kappa}l$. The reason for this is illustrated in Figure 8.7, which shows orbits in the quadrupoles for the *FD* and *DF* directions. In both cases, the orbit displacement is larger in the focusing section than in the defocusing section; therefore, the focusing action is stronger. Figure 8.7 also shows that the focal points in the *x* and *y* directions are not equal. An initially parallel beam is compressed to a line rather than a point in the image planes. A lens with this property is called *astigmatic*. The term comes from the Latin word *stigma*, meaning a small mark. A lens that focuses equally in both directions can focus to a point or produce a two-dimensional image. Such a lens is called *stigmatic*. The term anastigmatic is also used. Astigmatism in the doublet arises from the displacement term c_{11}. Although initially parallel orbits emerge from *FD* and *DF* doublets with the

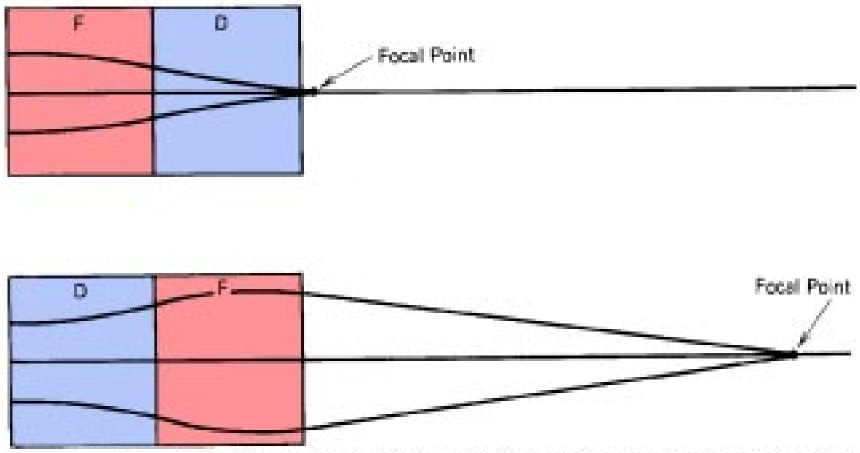

Figure 8.7 Astigmatism in a doublet lens. Orbits of particles initially parallel to the axis projected in the x and y planes.

same angle, the displacement is increased in the *DF* combination, and decreased in the *FD*.

The transfer matrix for a three-element optical system consisting of a drift space of length *l/2*, a thin lens with focal length *f*, and another drift space is

$$\mathbf{A} = \begin{bmatrix} 1 - l/2f & l - l^2/4f \\ -1/f & 1 - l/2f \end{bmatrix}. \tag{8.35}$$

Comparison of Eq. (8.35) with Eqs. (8.7) and (8.8) shows a correspondence if we take $f = \pm 1/\kappa l$. Thus, to order $(\sqrt{\kappa} l)^2$, quadrupole elements can be replaced by a drift space of length l with a thin lens at the center. This construction often helps to visualize the effect of a series of quadrupole lenses. A similar power series approximation can be found for the total ray transfer matrix of a doublet. Combining Eqs. (8.7) and (8.8) by matrix multiplication

$$\mathbf{C}_{DF} = \begin{bmatrix} 1 + \kappa l^2 & 2l \\ -2\kappa^2 l^3/3 & 1 - \kappa l^2 \end{bmatrix}. \tag{8.36}$$

$$\mathbf{C}_{FD} = \begin{bmatrix} 1 - \kappa l^2 & 2l \\ -2\kappa^2 l^3/3 & 1 + \kappa l^2 \end{bmatrix}. \tag{8.37}$$

Equations (8.36) and (8.37) are correct to order $(\sqrt{\kappa} l)^4$.

Stigmatism can be achieved with quadrupoles in a configuration called the triplet. This consists of three quadrupole sections. The entrance and exit sections have the same length ($l/2$) and pole orientation, while the middle section is rotated 90° and has length l. Orbits in the x and y planes of

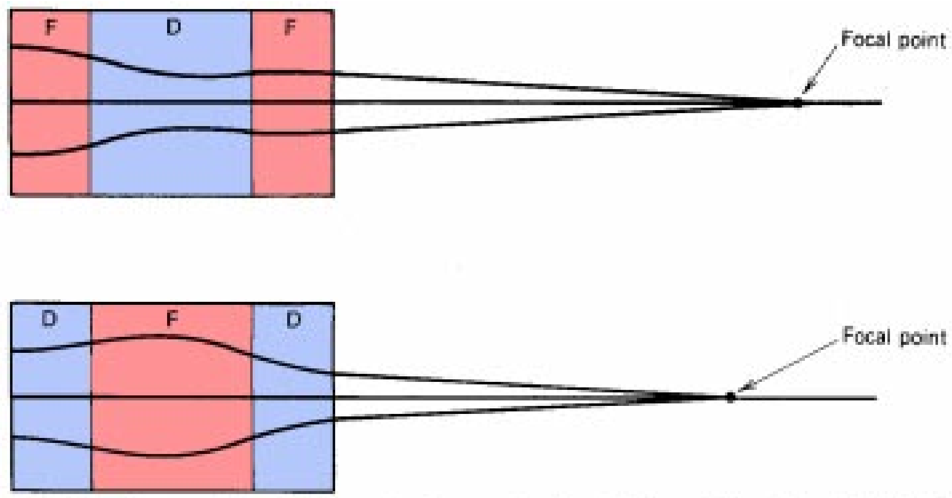

Figure 8.8 Improved stigmatic properties of a quadrupole triplet lens. Orbits of particles initially parallel to the axis projected in the x and y planes.

the triplet are illustrated in Figure 8.8. An exact treatment (using the trigonometric-hyperbolic forms of the transfer matrices) shows that the exit displacements are identical in both planes for equal entrance displacements. The power series expansions [Eqs. (8.7) and (8.8)] can be used to show that the exit angles are approximately equal. When the calculation is carried out, it is found that all terms of order $(\sqrt{\kappa}l)^2$ mutually cancel from the total matrix. The following result holds for both the *FDF* and *DFD* combinations:

$$\mathbf{C}_{triplet} = \begin{bmatrix} 1 & 2l \\ -\kappa^2 l^3/6 & 1 \end{bmatrix}. \tag{8.38}$$

Equation (8.38) is accurate to order $(\sqrt{\kappa}l)^4$.

8.5 FOCUSING IN A THIN-LENS ARRAY

As an introduction to periodic focusing, we shall study the thin-lens array illustrated in Figure 8.9. Orbits in this geometry can be determined easily. The focusing cell boundaries can have any location as long as they define a periodic collection of identical elements. We will take the boundary at the exit of a lens. A focusing cell consists of a drift space followed by a lens, as shown in Figure 8.9.

The goal is to determine the positions and angles of particle orbits at cell boundaries. The following equations describe the evolution of the orbit parameters traveling through the focusing cell labeled *(n+1)* in the series [see Eqs. (8.10) and (8.11)]. The subscript *n* denotes the orbit

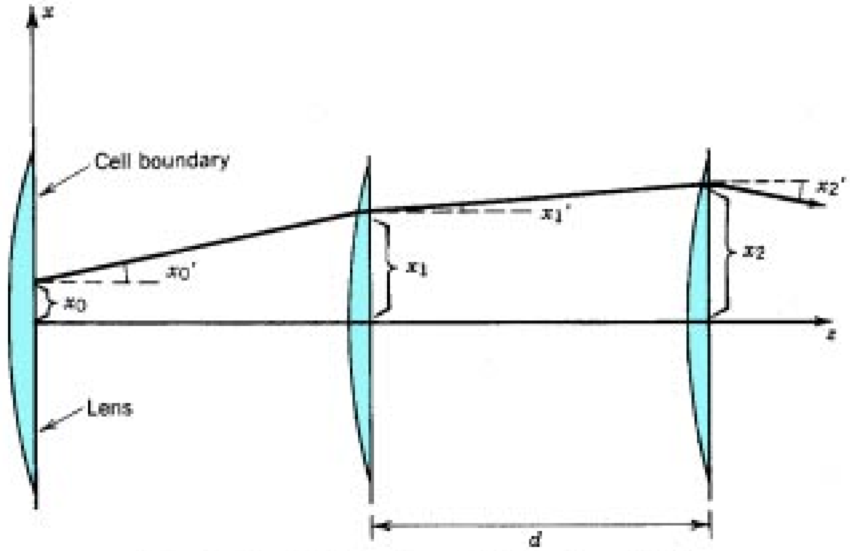

Figure 8.9 Particle orbit in first three cells of a uniform thin-lens array.

parameter at the exit of the *nth* focusing cell:

$$x_{n+1} = x_n + d x_n', \qquad (8.39)$$

$$x_{n+1}' = x_n' - x_{n+1}/f. \qquad (8.39)$$

Equation (8.39) can be solved for x_n'

$$x_n' = (x_{n+1} - x_n)/d. \qquad (8.41)$$

Equation (8.41) can be substituted in Eq. (8.40) to yield

$$x_{n+1}' = [(1-d/f)\ x_{n+1} - x_n]/d. \qquad (8.42)$$

Finally, an equation similar to Eq. (8.41) can be written for the transition through focusing cell *(n+2)*

$$x_{n+1}' = (x_{n+2} - x_{n+1})/d. \qquad (8.43)$$

Setting Eqs. (8.42) and (8.43) equal gives the difference equation

$$x_{n+2} - 2\ (1-d/2f)\ x_{n+1} + x_n = 0. \tag{8.44}$$

This is the finite difference equivalent of a second-order differential equation. We found in Section 4.2 that the finite difference approximation to the second derivative of a function involves the values of the function at three adjacent mesh points.

We seek a mathematical solution of Eq. (8.44) in the form

$$x_n = x_o\ \exp(jn\mu). \tag{8.45}$$

Defining $b = 1 - d/2f$ and substituting in Eq. (8.44),

$$\exp[j(n+2)\mu] - 2b\ \exp[j(n+1)\mu] + \exp(jn\mu) = 0, \quad \textit{or}$$
$$\exp(2j\mu) - 2b\ \exp(j\mu) + 1 = 0. \tag{8.46}$$

Applying the quadratic formula, the solution of Eq. (8.46) is

$$\exp(j\mu) = b \pm j\ \sqrt{1-b^2}. \tag{8.47}$$

The complex exponential can be rewritten as

$$\exp(j\mu) = \cos\mu + j\ \sin\mu = \cos\mu + j\ \sqrt{1-\cos^2\mu}\ . \tag{8.48}$$

Comparing Eqs. (8.47) and (8.48), we find that

$$\mu = \pm\cos^{-1}b = \pm\cos^{-1}(1-d/2f). \tag{8.49}$$

The solution of Eq. (8.47) is harmonic when $|b| \leq 1$. The particle displacement at the cell boundaries is given by the real part of Equation 8.45,

$$x_n = x_0\ \cos(n\mu+\varphi). \tag{8.50}$$

Equation (8.50) gives the displacement measured at a cell boundary. It does not imply that particle orbits between boundaries are harmonic. In the thin-lens array, it is easy to see that orbits are straight lines that connect the points of Eq. (8.45). The quantity μ is called the *phase advance* in a focusing cell. The meaning of the phase advance is illustrated in Figure 8.10. The case shown has $\mu = 2\pi/7 = 51.4°$. Particle orbits between cell boundaries in other focusing systems are generally not straight lines. Orbits in quadrupole lens arrays are more complex, as we will see in Section 8.7.

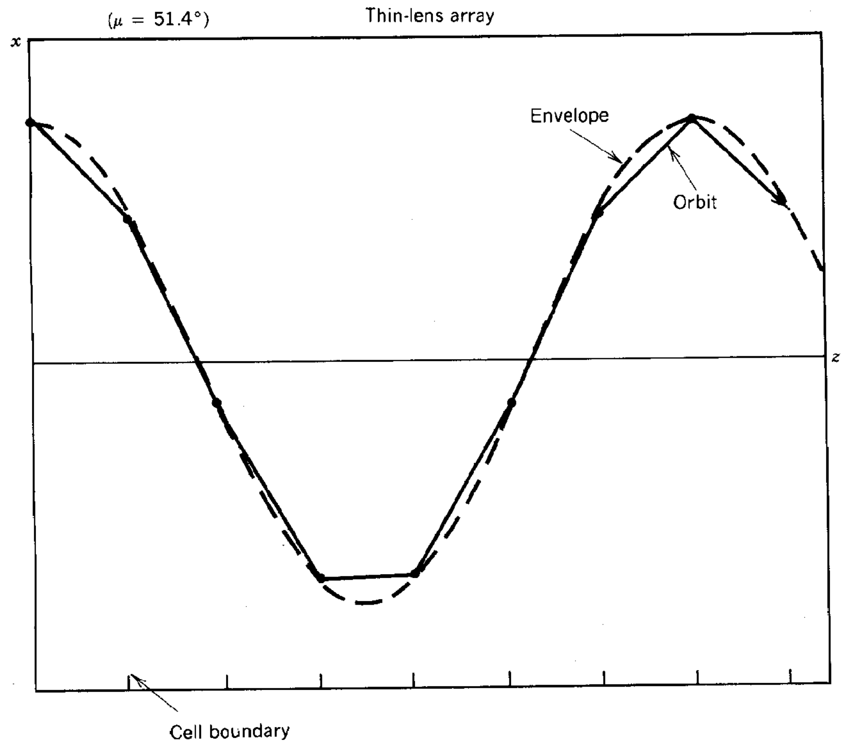

Figure 8.10 Particle orbit in a thin-lens array with phase advance per cell of 51.4°. Solid line: Actual particle orbit. Dotted line: Envelope function to calculate particle displacement at cell boundaries.

The orbit angle at cell boundaries can be determined by substituting Eq. (8.45)in Eq. (8.41). The result is

$$x_n' = (x_o/d)\ \big(\exp[j(n+1)\mu] - \exp(jn\mu)\big) = (x_o/d)\ \exp(jn\mu)\ [\exp(j\mu)-1]. \tag{8.51}$$

Note that when $\mu \Rightarrow 0$, particle orbits approach the continuous envelope function $x(z) = x_0\ \cos(\mu z/d+\varphi)$. In this limit, the last factor in Eq. (8.51) is approximately $j\mu$ so that the orbit angle becomes

$$x_n' = Re([jx_0\mu/d]\ [\exp(jn\mu)]) \cong -(x_0\mu/d)\ \sin(n\mu z/d). \tag{8.52}$$

An important result of the thin-lens array derivation is that there are parameters for which all particle orbits are unstable. Orbits are no longer harmonic but have an exponentially growing displacment when

$$|b| = |1-d/2f| \geq 1. \tag{8.53}$$

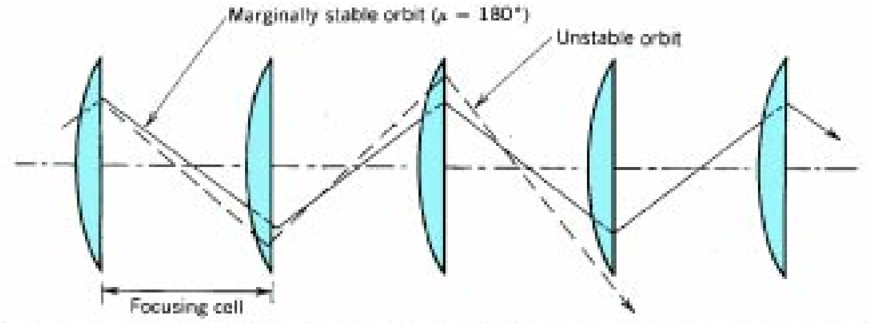

Figure 8.11 Orbital instability in a thin-lens array. Solid-line: Marginally stable orbit (μ → 180°). Dashed line: Unstable orbit resulting from a slight decrease of lens focal length.

Setting *1 - d/2f* equal to -1 gives the following stability condition for transport in a thin-lens array,

$$f \geq d/4 \quad (stability). \tag{8.54}$$

There is a maximum usable lens strength for a given cell length. The physical interpretation of this instability can be visualized by reference to Figure 8.11. The lens system has $f = d/4$ so that the particle orbit is marginally stable. In this case, $b = -1$ and $\mu = 180°$. The orbit crosses the boundary with a displacement of equal magnitude but opposite sign. If the focusing strength of the lens is increased slightly ($f < d/4$), then the particle has an increased magnitude of displacement at each cell boundary as shown by the dotted line. The amplitude of displacement increases without limit.

8.6 RAISING A MATRIX TO A POWER

We want to generalize the treatment of the previous section to investigate orbits and stability properties for any linear focusing system. Focusing cells may be complex in high-energy accelerators. They may include quadrupole lenses, bending magnets, gradient fields, and edge focusing. Nonetheless, the net effect of a focusing cell can be represented by a single 4 × 4 transfer matrix no matter how many sequential elements it contains. When transverse motions along Cartesian coordinates are decoupled, each direction is separately characterized by a 2 × 2 matrix.

A periodic focusing system consists of a series of identical cells. We shall restrict consideration to transport in the absence of acceleration. This applies directly to storage rings, beamlines, and electron confinement in a microwave tube. It is also a good approximation for accelerators if the betatron wavelength is short compared to the distance over which a particle's energy is doubled.

If a particle enters a periodic channel with an orbit vector $\mathbf{u}_0$, then the vector at the boundary between the first and second focusing cells is $\mathbf{u}_1 = \mathbf{C}\mathbf{u}_0$. The quantity $\mathbf{C}$ is the transfer matrix for a cell. After traversing *n* cells, the orbit vector is

$$\boldsymbol{u_n} = \boldsymbol{C}^n\, \boldsymbol{u_0}. \tag{8.55}$$

The quantity $\mathbf{C}^n$ denotes the matrix multiplication of **C** by itself *n* times. The behavior of particle orbits in periodic focusing systems is determined by the matrix power operation. In particular, if all components of $\mathbf{C}^n$ are bounded as $n \Rightarrow \infty$, then particle orbits are stable.

Analytic expressions for even small powers of a matrix can rapidly become unwieldy. The involved terms encountered in matrix multiplication are evident in Eqs. (8.33) and (8.34). We must use new methods of analysis to investigate the matrix power operation. We will concentrate on 2 × 2 matrices; the extension to higher-order matrices involves more algebra but is conceptually straightforward. We have already encountered the determinant of a matrix in Section 8.2. The determinant of a transfer matrix is always equal to unity when there is no acceleration. Another useful quantity is the *trace* of a matrix, defined as the sum of diagonal elements. To summarize, if

$$\boldsymbol{C} = \begin{bmatrix} c_{11} & c_{12} \\ c_{21} & c_{22} \end{bmatrix},$$

then

$$\det\boldsymbol{C} = c_{11}c_{22} - c_{12}c_{21} \tag{8.56}$$

and

$$Tr\ \boldsymbol{C} = c_{11} + c_{22}. \tag{8.57}$$

Transfer matrices have *eigenvalues* and *eigenvectors*. These quantities are defined in the following way. For most square matrices, there are orbit vectors and numerical constants that satisfy the equation

$$\boldsymbol{C}\ \mathbf{v}_i = \lambda_i\ \mathbf{v}_i. \tag{8.58}$$

The vectors for which Eq. (8.58) is true are called eigenvectors (characteristic vectors) of the matrix. The numerical constants (which may be complex numbers) associated with the vectors are called eigenvalues.

The following results are quoted without proof from the theory of linear algebra. The order of a square matrix is the number of rows (or columns). A square matrix of order *m* with nonzero determinant has *m* eigenvectors and *m* different eigenvalues. The eigenvectors have the property of *orthogonality*. Any *m*-dimensional orbit vector can be represented as a linear combination of eigenvectors. In the case of a 2 × 2 transfer matrix, there are two eigenvectors. Any orbit vector at the entrance to a periodic focusing system can be written in the form

$$\boldsymbol{u_0} = a_1\ \mathbf{v_1} + a_2\ \mathbf{v_2}. \tag{8.59}$$

If the orbit given by the input vector of Eq. (8.59) passes through n focusing cells of a periodic system, it is transformed to

$$\boldsymbol{u_0} = \boldsymbol{C}^n\ \boldsymbol{u_0} = a_1\ \lambda_1^n\ \mathbf{v_1} + a_2\ \lambda_2^n\ \mathbf{v_2}. \tag{8.60}$$

Equation (8.60) demonstrates the significance of the eigenvector expansion for determining the power of a matrix. The problem of determining the orbit after a large number of focusing cells is reduced to finding the power of two numbers rather than the power of a matrix. If λ_1^n and λ_2^n are bounded quantities for $n \gg 1$, then orbits are stable in the focusing system characterized by the transfer matrix **C**.

The eigenvalues for a 2 x 2 matrix can be calculated directly. Writing Eq. (8.58) in component form for a general eigenvector *(v,v')*,

$$(c_{11}-\lambda)\ \nu + c_{12}\ \nu' = 0, \tag{8.61}$$

$$c_{21}\ \nu + (c_{22}-\lambda)\ \nu' = 0. \tag{8.62}$$

Multiplying Eq. (8.62) by $c_{12}/(c_{22}-\lambda)$ and subtracting from Eq. (8.61), we find that

$$\frac{(c_{11}-\lambda)\ (c_{22}-\lambda) - c_{12}c_{21}}{(c_{22}-\lambda)}\ \nu = 0. \tag{8.63}$$

Equation (8.63) has a nonzero solution when

$$(c_{11}-\lambda)\ (c_{22}-\lambda) - c_{12}c_{21} = 0. \tag{8.64}$$

This is a quadratic equation that yields two values of λ. The values can be substituted into Eq. (8.61) or (8.62) to give v_1' in terms of v_1 and v_2' in terms of v_2. Equation (8.64) can be rewritten

$$\lambda^2 - \lambda\ Tr\boldsymbol{C} + \det\boldsymbol{C} = 0. \tag{8.65}$$

The solution to Eq. (8.65) can be found from the quadratic formula using the fact that $det\boldsymbol{C} = 1$.

$$\lambda_1,\lambda_2 = (Tr\boldsymbol{C}/2) \pm \sqrt{(Tr\boldsymbol{C}/2)^2-1}. \tag{8.66}$$

The product of the two eigenvalues of Eq. (8.66) is

$$\lambda_1 \lambda_2 = (Tr\boldsymbol{C}/2)^2 - [(Tr\boldsymbol{C}/2)^2 - 1] = 1. \tag{8.67}$$

The fact that the product of the eigenvalues of a transfer matrix is identically equal to unity leads to a general condition for orbital stability. We know that the eigenvalues are different if *det**C*** and *Tr**C*** are nonzero. If both eigenvalues are real numbers, then one of the eigenvalues must have a magnitude greater than unity if the product of eigenvalues equals 1. Assume, for instance, that $\lambda_1 > 1$. The term λ_1 will dominate in Eq. (8.60). The magnitude of the orbit displacement will diverge for a large number of cells so that orbits are unstable. Inspecting Eq. (8.65), the condition for real eigenvalues and instability is $|Tr\boldsymbol{C}/2| > 1$.

When $|Tr\boldsymbol{C}/2| \leq 1$, the square root quantity is negative in Eq. (8.65) so that the eigenvalues are complex. In this case, Eq. 8.66 can be rewritten

$$\lambda_1, \lambda_2 = (Tr\boldsymbol{C}/2) \pm j \sqrt{1-(Tr\boldsymbol{C}/2)^2}. \tag{8.68}$$

If we make the formal substitution

$$Tr\boldsymbol{C}/2 = \cos\mu, \tag{8.69}$$

then Eq. (8.68) becomes

$$\lambda_1, \lambda_2 = \cos\mu \pm j \sin\mu = \exp(\pm j\mu).. \tag{8.70}$$

Euler's formula was applied to derive the final form. The eigenvalues to the *n*th power are $exp(\pm nj\mu)$. This is a periodic trigonometric function. The magnitude of both eigenvalues is bounded for all powers of *n*. Thus, the orbit displacement remains finite for $n \Rightarrow \infty$ and the orbits are stable. To reiterate, if the action of a cell of a periodic focusing system is represented by a transfer matrix **C**, then orbits are stable if

$$|Tr\boldsymbol{C}/2| \leq 1 \quad (stability). \tag{8.71}$$

This simple rule holds for any linear focusing cell.

We have concentrated mainly on mathematics in this section. We can now go back and consider the implications of the results. The example of the drift space and thin lens will be used to illustrate application of the results. The transfer matrix is

$$\boldsymbol{C} = \begin{bmatrix} 1 & d \\ -1/f & 1-d/f \end{bmatrix}. \tag{8.72}$$

The determinant is equal to unity. The trace of the matrix is $Tr\boldsymbol{C} = 2-d/f$. Applying Eq. (8.71), the condition for stable orbits is

$$|1-d/2f| \leq 1, \tag{8.73}$$

as we found before. Similarly, $\cos\mu = 1-d/2f$. Thus, the parameter μ has the same value as Eq. (8.49) and is associated with the phase advance per cell. This holds in general for linear systems. When the orbits are stable and the eigenvalues are given by Eq. (8.70), the orbit vector at the cell boundaries of any linear focusing cell is

$$\boldsymbol{u_n} = a_1 \nu_1 \exp(jn\mu) + a_2 \nu_2 \exp(-jn\mu). \tag{8.74}$$

The solution is periodic; orbits repeat after passing through $N = 2\pi/\mu$ cells.

The eigenvectors for the transfer matrix [Eq. (8.72)] can be found by substituting the eigenvalues in Eq. (8.61). The choice of ν is arbitrary. This stands to reason since all orbits in a linear focusing system are similar, independent of magnitude, and the eigenvectors can be multiplied by a constant without changing the results. Given a choice of the displacement, the angle is

$$\nu' = (\lambda-c_{11})\ \nu\ /\ c_{12}. \tag{8.75}$$

The eigenvectors for the thin-lens array are

$$\boldsymbol{\nu_1} = (\ 1, [\exp(j\mu)-1]/d\ ), \tag{8.76}$$

$$\boldsymbol{\nu_2} = (\ 1, [\exp(-j\mu)-1]/d\ ), \tag{8.77}$$

Suppose we wanted to treat the same orbit considered in Section 8.5 [Eq. (8.45)]. The particle enters the first cell parallel to the axis with a displacement equal to x_0. The following linear combination of eigenvectors is used.

$$\boldsymbol{u_o} = x_0\ \boldsymbol{\nu_1}. \tag{8.78}$$

The displacement after passing through n cells is

$$x_n = x_0\ Re[\exp(jn\mu)] = x_0 \cos(n\mu). \tag{8.79}$$

as we found from the finite difference solution. The angle after n cells is

$$x_n' = x_0 \exp(jn\mu)\ [\exp(j\mu)-1]/d. \tag{8.80}$$

The expression is identical to Eq. (8.51). Both models lead to the same conclusion. We can now proceed to consider the more complex but practical case of *FD* quadrupole focusing cells.

8.7 QUADRUPOLE FOCUSING CHANNELS

Consider the focusing channel illustrated in Figure 8.12. It consists of a series of identical, adjacent quadrupole lenses with an alternating 90' rotation. The cell boundary is chosen so that the cell consists of a defocusing section followed by focusing section (*DF*) for motion in the *x* direction. The cell is therefore represented as *FD* in the *y* direction. Note that individual lenses do not comprise a focusing cell. The smallest element of periodicity contains both a focusing and a defocusing lens. The choice of cell boundary is arbitrary. We could have equally well chosen the boundary at the entrance to an *F* lens so that the cell was an *FD* combination in the *x* direction. Another valid choice is to locate the boundary in the middle of the *F* lens so that focusing cells are quadrupole triplets, *FDF*. Conclusions related to orbital stability do not depend on the choice of cell boundary.

The transfer matrix for a cell is the product of matrices $\mathbf{C} = \mathbf{A}_F\mathbf{A}_D$. The individual matrices are given by Eqs. (8.4) and (8.6). Carrying out the multiplication,

$$\boldsymbol{C} = \begin{bmatrix} \cos\Gamma\cosh\Gamma + \sin\Gamma\sinh\Gamma & (\cos\Gamma\sinh\Gamma + \sin\Gamma\cosh\Gamma)/\sqrt{\kappa} \\ \sqrt{\kappa}(\cos\Gamma\sinh\Gamma - \sin\Gamma\cosh\Gamma) & \cos\Gamma\cosh\Gamma - \sin\Gamma\sinh\Gamma \end{bmatrix}. \tag{8.81}$$

where $\Gamma = \sqrt{\kappa}l$. Taking $|Tr\boldsymbol{C}/2| < 1$ the condition for stable orbits is

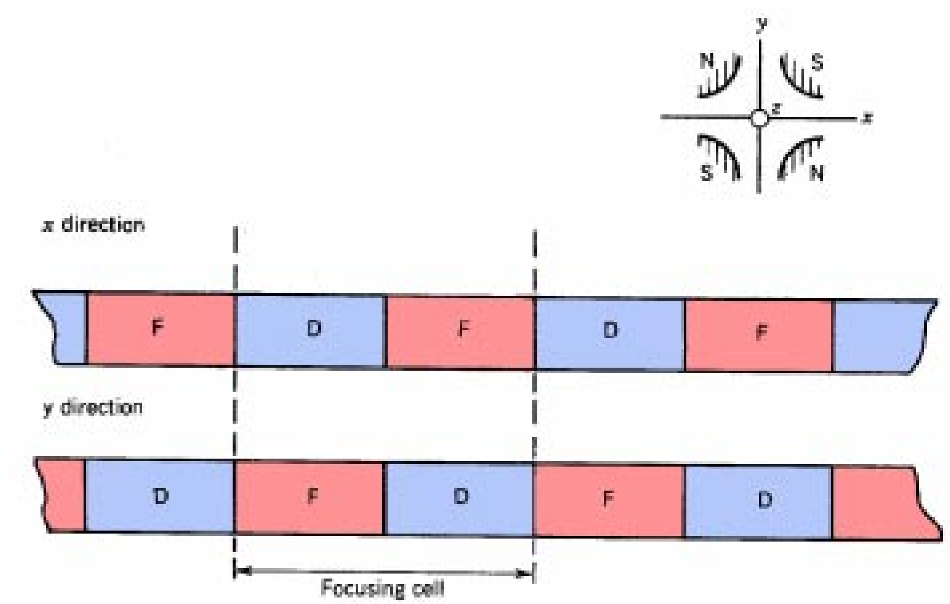

Figure 8.12 Array of quadrupole lenses in an FD configuration. Action of lenses indicated for motion in *x* and *y* directions.

$$-1 \leq \cos\Gamma \cosh\Gamma \leq +1. \tag{8.82}$$

Figure 8.13 shows a plot of $f(\Gamma) = \cos\Gamma \cosh\Gamma$ versus Γ. Only positive values of Γ have physical meaning. Orbits are stable for Γ in the range

$$0 \leq \Gamma \leq 1.86. \tag{8.83}$$

A stable orbit (calculated by direct solution of the equation of motion in the lens fields) is plotted in Figure 8.14a. The orbit has $\Gamma = 1$, so that $\mu = 0.584 = 33.5°$. Higher values of Γ correspond to increased lens strength for the same cell length. Orbits are subject to the same type of overshoot instability found for the thin-lens array [Eq. (8.53)]. An unstable orbit with $\Gamma = 1.9$ is plotted in Figure 8.14b. At higher values of Γ, there are regions of Γ in which stable propagation can occur. Figure 8.14c illustrates a stable orbit with $\Gamma = 4.7$ ($\mu = 270°$). Orbits such as those of Figure 8.14c strike a fragile balance between focusing and defocusing in a narrow range of Γ. Higher-order stability bands are never used in real transport systems. For practical purposes, Γ must be in the range indicated by Eq. (8.83). The same result applies to motion in the *y*

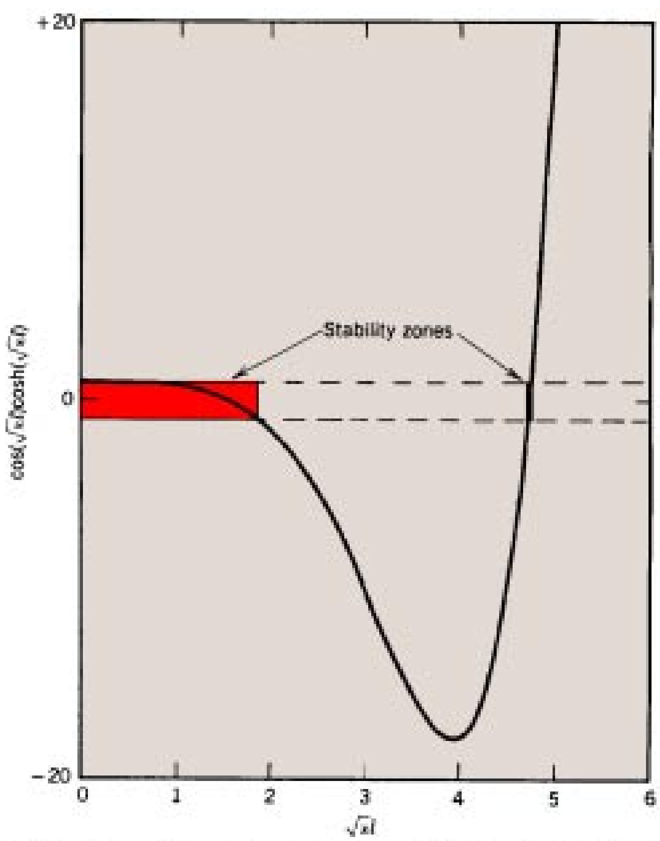

Figure 8.13 Orbital stability in an FD quadrupole array. Plot of $\cos(\sqrt{\kappa}\, l)\cosh(\sqrt{\kappa}\, l)$ versus $\sqrt{\kappa}\, l$.

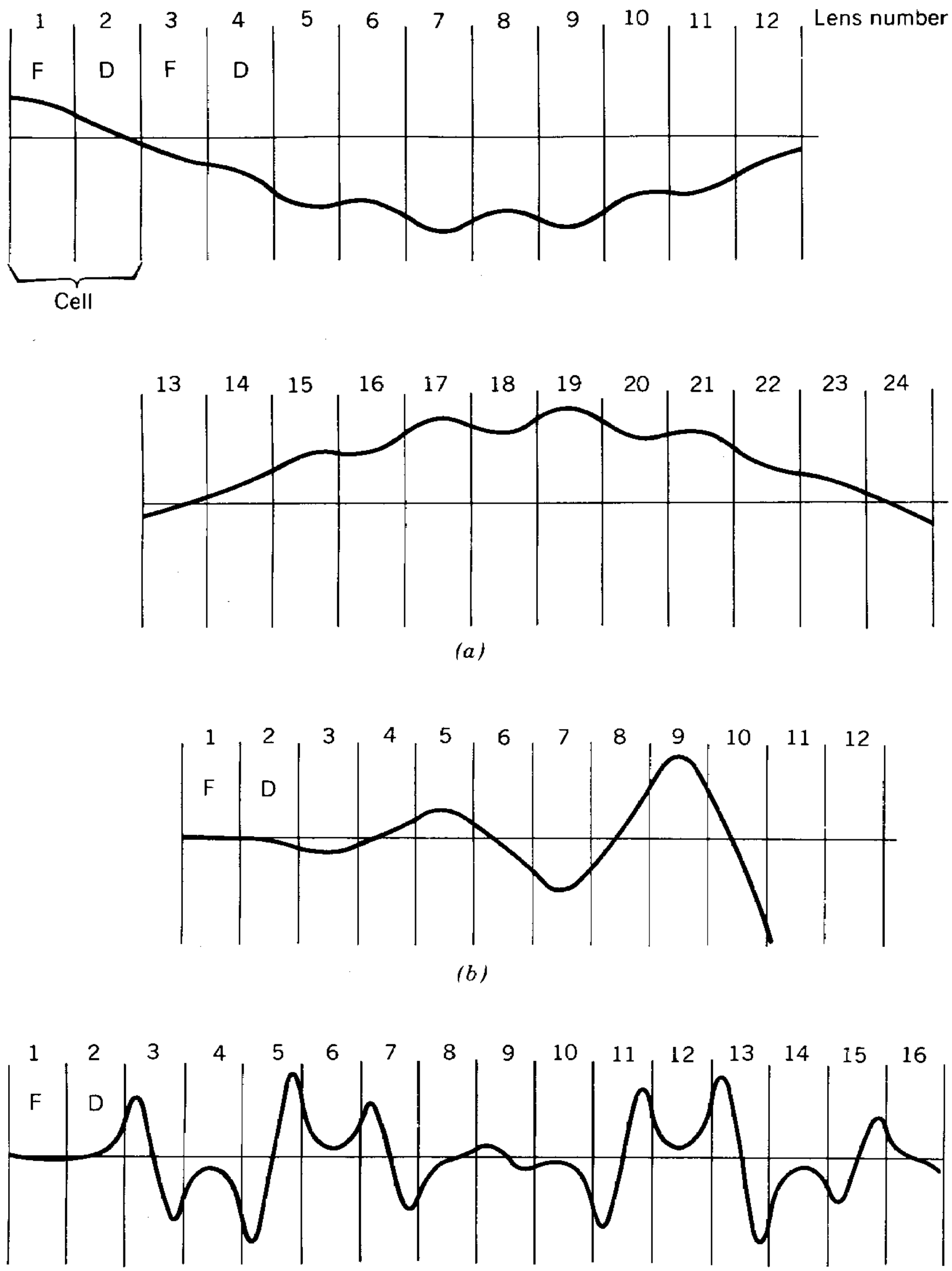

Figure 8.14 Numerical calculations of actual particle orbits in an FD quadrupole array. (*a*) $\sqrt{\kappa}\, l = 1$ (stable orbit, first passband). (*b*) $\sqrt{\kappa}\, l = 1.9$ (unstable orbit). (*c*) $\sqrt{\kappa}\, l = 4.7$ (stable orbit, second passband).

direction. The matrix coefficients are different from those of Eq. (8.81), but the quantity *Tr**C**/2* is the same.

Given a range of Γ for stable operation, it remains to determine an optimum value. Small phase advance ($\mu \ll 1$) has advantages. The effect of any one lens is small so that orbits approach the continuous focusing limit (Section 7.1). Beam envelope oscillations in a cell are small, and particle orbits are less affected by errors and misalignments of the lenses. Small μ is an effective choice for an array of lenses with positive focal length, such as the thin-lens array discussed in Section 8.5. The thin-lens array is a good model for a series of solenoidal magnetic lenses or unipotential electrostatic lenses. In such lens arrays, we can show that to first order the focusing strength is independent of μ for given applied fields. The focusing strength is proportional to the average transverse force that the lenses exert on the particles [Eq. (7.6)]. Neglecting edge fields, the focal length of a solenoidal lens is inversely proportional to the length of the lens, d. Thus, the product fd in Eq. (7.6) does not depend on the number of individual lenses per unit axial length. In other words, given a series of solenoids with phase advance μ, focal length f, and lens length d, the acceptance would be unchanged if the lens length and phase advance were halved and the focal length were doubled. Thus, it is generally best to use small phase advance and a fine division of cells in channels with only focusing lenses. The minimum practical cell length is determined by ease of mechanical construction and the onset of nonlinearities associated with the edge fields between lenses.

This conclusion does not apply to *FD*-type focusing channels. In order to investigate scaling in this case, consider the quadrupole doublet treated using the expansions for small $\sqrt{\kappa} l$ [Eqs. (8.7), (8.8), and (8.35)]. In this approximation, the doublet consists of two lenses with focal lengths

$$f_F = +1/\kappa l, \qquad f_D = -1/\kappa l,$$

separated by a distance l. As with the solenoidal lens, the focal lengths of the individual lenses are inversely proportional to the lengths of the lens. The net positive focal length of the combination from Eqs. (8.36) and (8.37) is

$$f_{FD} = 3/2\kappa^2 l^3 = 3|\, f_F\, f_D\,|/2l \sim 1/d^3. \tag{8.84}$$

where $d = 2l$ is the cell length.

If we divide the quadrupole doublet system into smaller units with the same applied field, the scaling behavior is different from that of the solenoid channel. The average focusing force decreases, because the product $f_{FD}d$ is proportional to d^{-2} . This scaling reflects the fact that the action of an *FD* combination arises from the difference in average radius of the orbits in the *F* and *D* sections. Dividing the lenses into smaller units not only decreases the focusing strength of the *F* and *D* sections but also reduces the relative difference in transverse displacement. The conclusion is that *FD* focusing channels should be designed for the highest acceptable value of phase advance. The value used in practice is well below the stability limit. Orbits in channels with high μ are sensitive to misalignments and field errors. A phase advance of $\mu = 60^\circ$ is usually used.

In many strong focusing systems, alternate cells may not have the same length or focusing strength. This is often true in circular accelerators. This case is not difficult to analyze. Defining $\Gamma_1 = \sqrt{\kappa_1}\ l_1$ and $\Gamma_2 = \sqrt{\kappa_2}\ l_2$, the transfer matrix for motion in the *DF* direction is

$$\boldsymbol{C} = \begin{bmatrix} \cos\Gamma_1 & \sin\Gamma_1/\sqrt{\kappa_1} \\ -\sqrt{\kappa_1}\sin\Gamma_1 & \cos\Gamma_1 \end{bmatrix} \begin{bmatrix} \cosh\Gamma_1 & \sinh\Gamma_1/\sqrt{\kappa_1} \\ \sqrt{\kappa_1}\sinh\Gamma_1 & \cosh\Gamma_1 \end{bmatrix}. \tag{8.85}$$

Performing the matrix multiplication and taking *Tr**C**/2* gives the following phase advance:

$$\cos\mu_{DF} = \cos\Gamma_1\ \cosh\Gamma_2 + \left(\frac{\sin\Gamma_1\ \sinh\Gamma_2}{2}\right)\left(\frac{\Gamma_2 l_1}{\Gamma_1 l_2} - \frac{\Gamma_1 l_2}{\Gamma_2 l_1}\right). \tag{8.86}$$

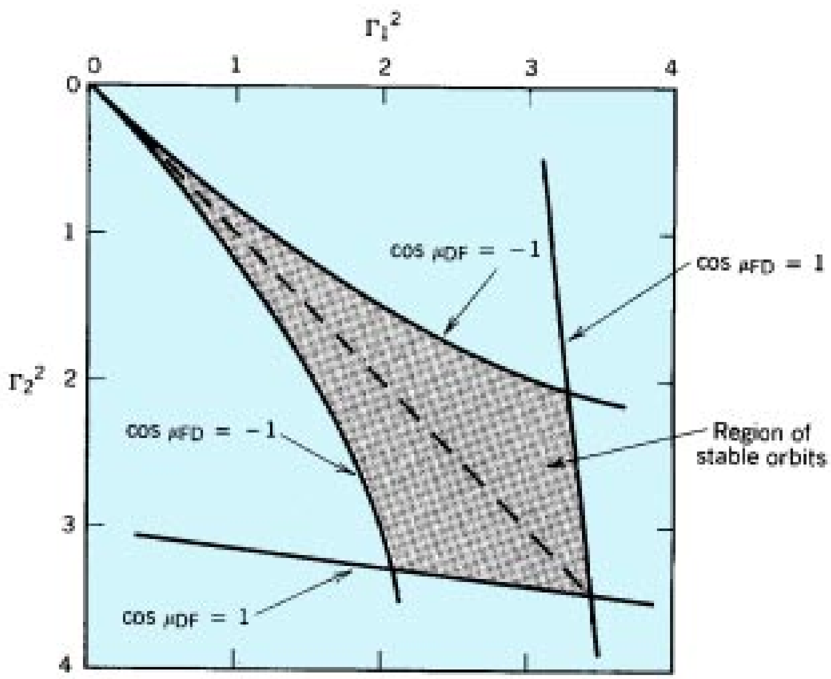

Figure 8.15 Necktie diagram. Orbital stability in an FD (DF) quadrupole array; the two lenses of a cell have unequal focusing strength. $\Gamma_1 = \sqrt{\kappa_1}\, l_1$, $\Gamma_2 = \sqrt{\kappa_2}\, l_2$. Region of parameter space with orbital stability in both x and y directions shaded. FD (lens 1 focusing, lens 2 defocusing). DF (lens 1 defocusing, lens 2 focusing).

Because the two lenses of the cell have unequal effects, there is a different phase advance for the *FD* direction, given by

$$\cos\mu_{FD} = \cosh\Gamma_1 \cos\Gamma_2 + \left(\frac{\sinh\Gamma_1 \sin\Gamma_2}{2} \right) \left(\frac{\Gamma_1 l_2}{\Gamma_2 l_1} - \frac{\Gamma_2 l_1}{\Gamma_1 l_2} \right) . \tag{8.87}$$

There is little difficulty deriving formulas such as Eqs. (8.86) and (8.87). Most of the problem is

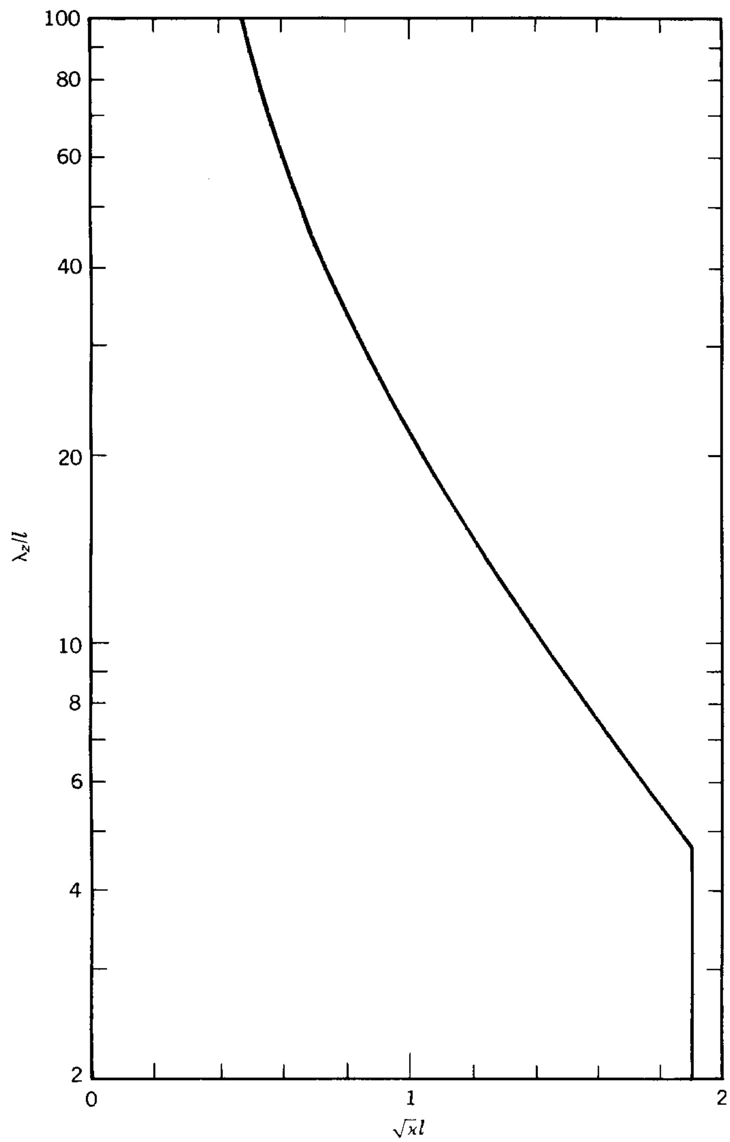

Figure 8.16 Betatron wavelength in a quadrupole focusing channel normalized to the length of a lens as a function of $\sqrt{\kappa_2}\,l$. FD channel with uniform lenses.

centered on plotting and interpreting the results. There are conditions in two directions that must be satisfied simultaneously for stable orbits:

$$-1 \leq \cos\mu_{FD} \leq +1, \qquad (8.88)$$

$$-1 \leq \cos\mu_{DF} \leq +1. \qquad (8.89)$$

The stability results are usually plotted in terms of Γ_1^2 and Γ_2^2 in a diagram such as Figure 8.15. This region of parameter space with stable orbits is shaded. Figure 8.15 is usually called a "necktie" diagram because of the resemblance of the stable region to a necktie, circa 1952. The shape of the region depends on the relative lengths of the focusing and defocusing lenses. The special case we studied with equal lens properties is a 45° line on the $1_1 = 1_2$ diagram. The maximum value of Γ^2 is $(1.86)^2$. An accelerator designer must ensure that orbits remain well within the stable region for all regimes of operation. This is a particular concern in a synchrotron

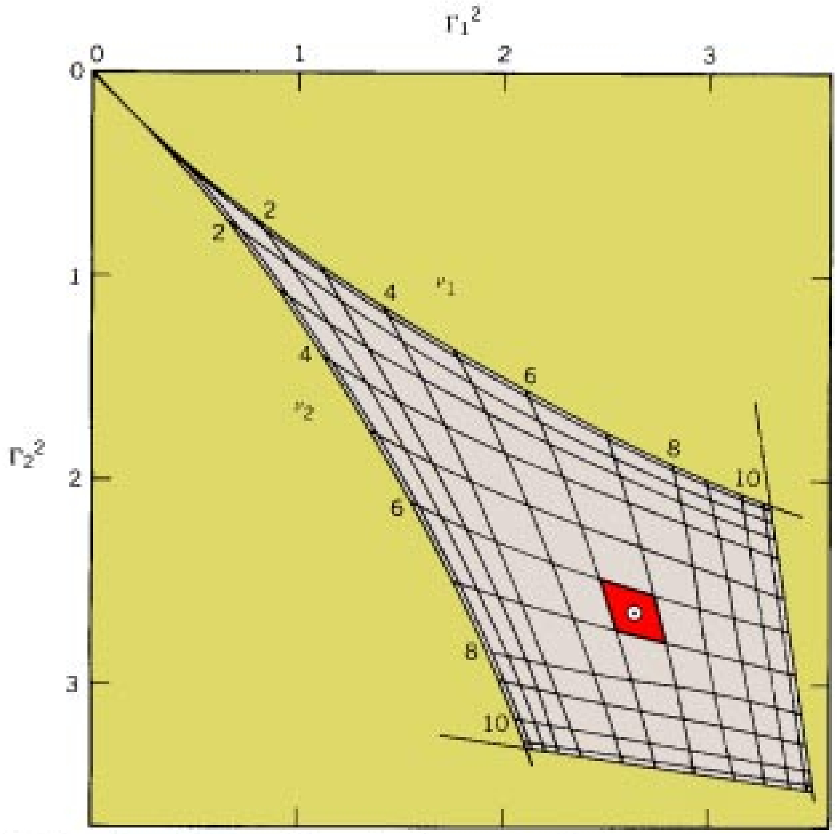

Figure 8.17 Beam focusing by an FD quadrupole array in a circular accelerator. Necktie diagram with conditions for orbital resonances included (24 cells per revolution). Possible operating point indicated at ν = 6.4. (M. S. Livingston and J. P. Blewett, *Particle Accelerators*, used by permission, McGraw-Hill Book Co.).

where the energy of particles and strength of the focusing field varies during the acceleration cycle.

The betatron wavelength for orbits in a quadrupole channel is

$$\lambda_z = (2\pi d/\mu), \tag{8.90}$$

where d is the cell length and $d = 21$. When F and D cells have the same parameters, Eq. (8.90) can be written

$$\lambda_z = \frac{2\pi d}{\cos^{-1}(\cos\Gamma\cosh\Gamma)} . \tag{8.91}$$

The quantity λ_z/l is plotted in Figure 8.16 as a function of Γ. The betatron wavelength is Important in circular machines. Particles may suffer resonance instabilities when the circumference of the accelerator or storage ring is an integral multiple of the betatron wavelength (Section 7.3). If we include the possibility of different focusing properties in the horizontal and verticle directions, resonance instabilities can occur when

$$\mu_{DF} = 2\pi n \ (d/C) \tag{8.92}$$

or

$$\mu_{FD} = 2\pi n \ (d/C) \tag{8.93}$$

with n = 1,2,3,4,... . Equations (8.92) and (8.93) define lines of constant $\cos\mu_{DF}$ or $\cos\mu_{FD}$, some of which are inside the region of general orbital stability. These lines, are included in the necktie diagram of Figure 8.17. They have the same general orientation as the lines $\cos\mu_{DF}$ = -1 or $\cos\mu_{FD}$= +1. The main result is that particle orbits in a circular machine with linear *FD* forces must remain within a quadrilateral region of Γ_1-Γ_2 space. If this is not true over the entire acceleration cycle, orbital resonance instabilities may occur with large attendant particle losses.